

Supplementary Materials

Geometrical and Magnetic Properties of Small Titanium and Chromium Clusters on Monolayer Hexagonal Boron Nitride

Dong Hao^{1,2}, Yueyi Wang², Xiangqian Tang^{1,2}, Xinjia Zhao¹, Yang An^{1,2}, Wenyu
Wang^{1,2}, Jianmei Li⁵, Xinyan Shan^{1,2,4}, Xinghua Lu^{1,2,3,4*}

¹Beijing National Laboratory for Condensed Matter Physics, Institute of Physics, Chinese
Academy of Sciences, Beijing 100190, China

²School of Physical Sciences, University of Chinese Academy of Sciences, Beijing 100190,
China

³Collaborative Innovation Center of Quantum Matter, Beijing 100190, China

⁴Songshan Lake Materials Laboratory, Dongguan, Guangdong 523808, China

⁵Key Laboratory for Microstructural Material Physics of Hebei Province, School of Science,
Yanshan University, Qinhuangdao, Hebei 066004, China

*Corresponding authors: xhlu@aphy.iphy.ac.cn

(1) Optimization of the h-BN

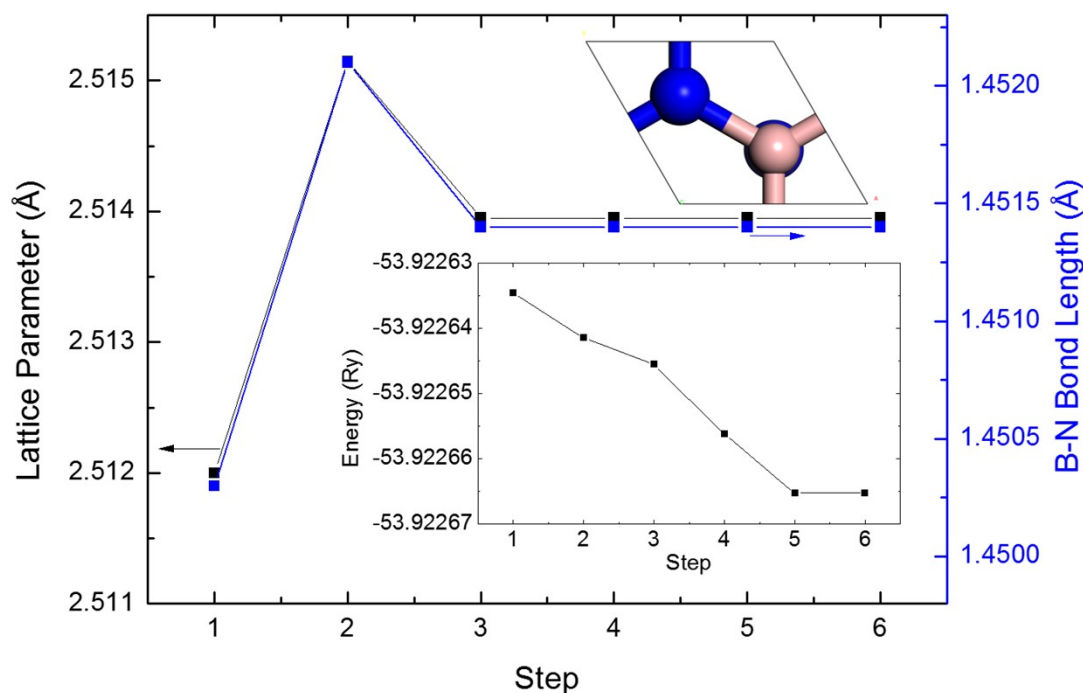


Figure S1. The optimization of the h-BN cell. The initial structural parameters of the hexagonal h-BN are obtained from the Materials Project (MP). The magnetic properties of TM clusters are strongly dependent on the final lattice

parameters of the substrate.

(2) Phonon spectrum and density of phonon states of Ti_3 cluster on h-BN

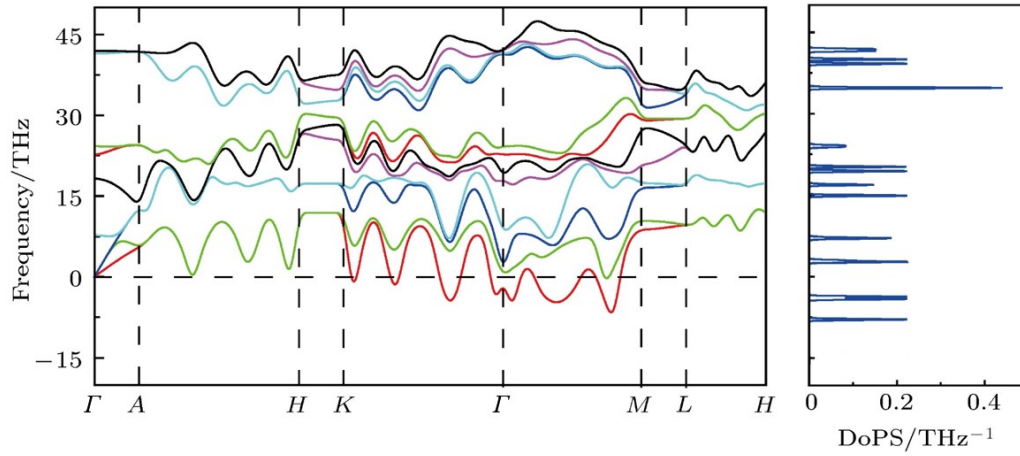


Figure S2. Phonon spectrum and density of phonon states of Ti_3 cluster on h-BN. For Cr_3 cluster on h-BN, the phonon dispersion curves are roughly the same. In the region between K and M point of the Brillouin zone, a few imaginary phonon modes emerge, perhaps derived from the weak interaction of the clusters in the adjacent periodic cells. Despite this subtle error, the adsorption system is dynamically stable.

(3) Magnetization of adsorbed Ti clusters

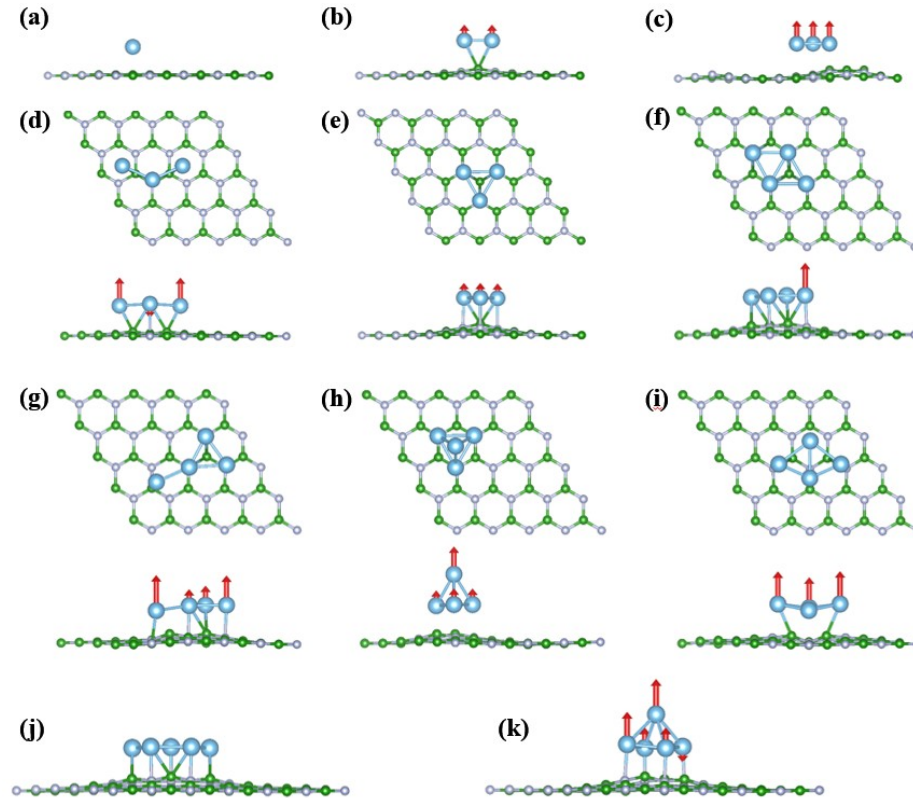


Figure S3. Geometries and magnetization of Ti_n ($n = 1, 2, 3, 4, 5$) clusters on

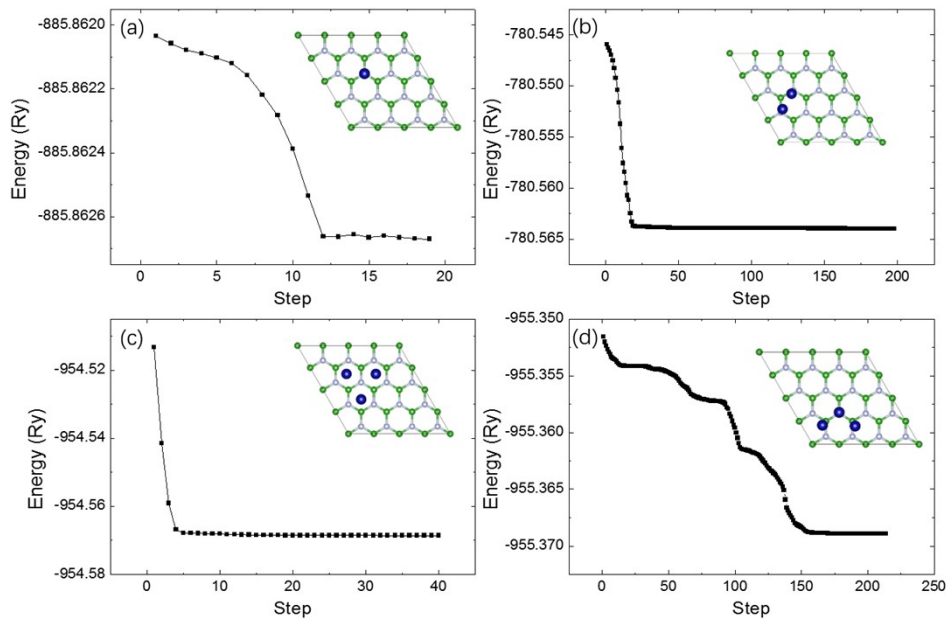
the relaxed h-BN supercell, top and side views. **(a)** Ti monomer, **(b)** Ti dimer, **(c)-(e)** Ti trimer, **(f)-(i)** Ti tetramer, and **(j)-(k)** Ti pentamer. Red arrows stand for magnetization of Ti atoms. These structures correspond to Fig. 1 and Table 1. Top views of (a)-(c) and (j)-(k) are shown in the main text. Silvery, green and blue balls represent N, B and Ti atoms, respectively.

The magnetization of adsorbed Ti clusters are shown in Fig. S3. Both collinear and noncollinear spin polarization SCF calculation are performed, and most noncollinear calculations converge to the collinear states. For simplicity, only the lowest-energy magnetic configurations of each geometry are given.

(4) Convergence in Computation of Cr_n ($n = 1, 2, 3, 4$) Clusters on h-BN

Figure S4 shows the convergence of Cr_n ($n=1,2,3,4$) clusters adsorbed on monolayer h-BN. The optimization steps increase quickly from 19 to 220 as the number of Cr atoms increase from 1 to 3, except for the noncollinear Cr trimer in which the initial (nearly) C_3 symmetric geometry renders a quick convergence.

The converge issue on the supported clusters of Cr_4 is investigated. At the first attempt, the hybrid TPSS meta-GGA functional is applied, along with the norm-conserving pseudopotential (NCP) scheme. The energy cutoff is set from 1360 up to 2720 eV to ensure the convergence. The second attempt is the Bayesian error estimate (BEE) functional. We consider Cr_4 on h-BN with a regular tetrahedron geometry and different magnetic configurations as starting points including collinear and noncollinear, ferromagnetic, antiferromagnetic and ferromagnetic. Unfortunately, both efforts have failed due to extremely slow convergence or oscillation in many electronic bands. Fig. S4(e) shows an example of the non-convergence. The origin of such nonconvergence may be the large value of the adsorption height (3.18 Å) of Cr_4 on h-BN which is 1.06 Å larger than that of Cr_4 on Cu(111), hence much weaker hybridization with the orbitals of the substrate atoms.



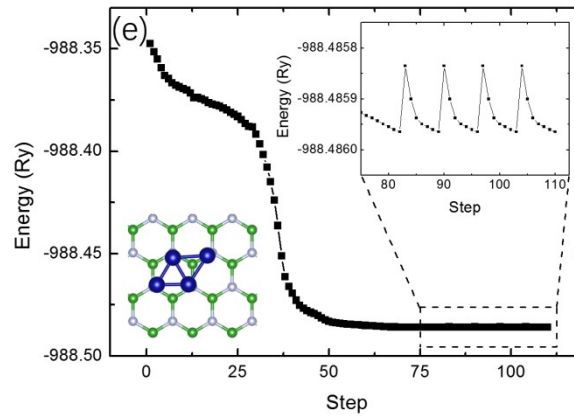


Figure S4. Convergence in computation of Cr_n clusters on h-BN surface. (a) Cr monomer, (b) Cr dimer, (c) and (d) Cr trimers with noncollinear and collinear magnetization. Insets: top view of the optimized geometries. (e) Cr tetramer. Insets: initial geometry (top view) for the computations.

(5) Bond lengths and coordinates of stable geometries of Ti/Cr clusters

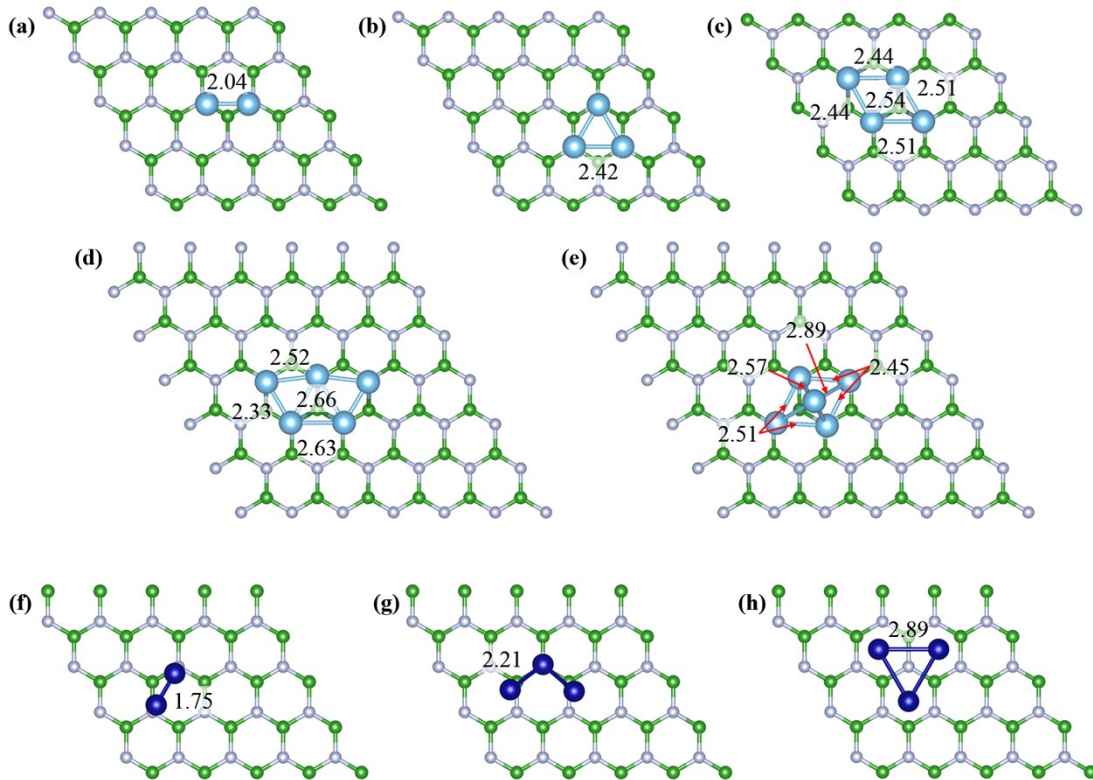


Figure S5. The bond lengths of stable geometries of Ti [(a)-(e)] and Cr [(f)-(h)] clusters on h-BN. The corresponding atomic coordinates of the clusters are listed in Table S1.

Table S1. The atomic coordinates of the Ti/Cr clusters in Figure S5.

Geometry	Atom	x	y	z
Fig. S5(a)	Ti ₁	4.3354256	5.7019085	8.45460
	Ti ₂	6.3737818	5.7040118	8.45508

Fig. S5(b)	Ti ₁	4.2116028	5.8568560	8.41284
	Ti ₂	1.7879812	5.8567308	8.41284
	Ti ₃	1.7879812	3.4332344	8.41296
Fig. S5(c)	Ti ₁	6.6955708	8.3254244	8.35584
	Ti ₂	9.1464860	8.3954112	8.43120
	Ti ₃	6.6253336	5.8747596	8.43132
	Ti ₄	9.1890540	5.8308144	8.43732
Fig. S5(d)	Ti ₁	4.9636291	7.3709246	2.53704
	Ti ₂	4.9959307	5.0548248	2.61624
	Ti ₃	9.9733819	7.3710749	2.53752
	Ti ₄	7.6424083	7.7185800	2.59620
	Ti ₅	7.6251307	5.0549750	2.61648
Fig. S5(e)	Ti ₁	7.6333939	6.2803325	4.77192
	Ti ₂	5.1433162	5.0364955	2.84136
	Ti ₃	9.9260563	7.4275651	2.67468
	Ti ₄	7.5657859	7.6015430	2.59284
	Ti ₅	7.5657859	4.8936173	2.59164
Fig. S5(f)	Cr ₁	3.8035760	5.4744451	12.1383
	Cr ₂	2.0468698	3.7305594	12.1435
Fig. S5(g)	Cr ₁	1.9889773	2.0997542	12.3741
	Cr ₂	4.2539955	3.4750512	11.3967
	Cr ₃	4.9992861	1.9812650	12.3748
Fig. S5(h)	Cr ₁	6.0980413	6.8051709	12.18546
	Cr ₂	3.2109293	6.8049706	12.18546
	Cr ₃	3.2109293	3.9180589	12.18546

(6) Spin-resolved Charge Density Difference in Ti_n Clusters

The spin-resolved charge density differences in Ti_n clusters are plotted in Fig. S6. Top row: spin up; bottom row: spin down.

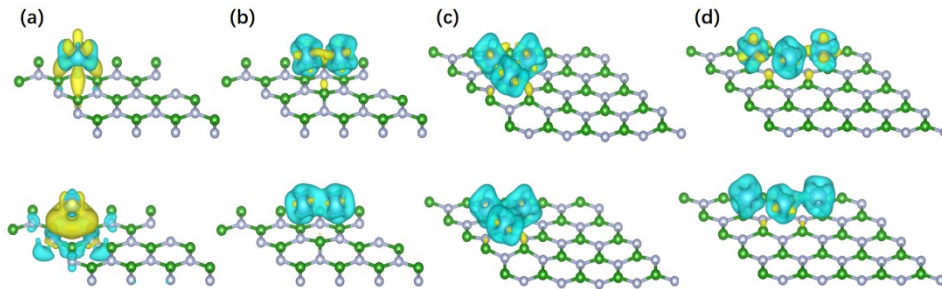


Figure S6. Spin-resolved charge density difference in Ti_n clusters, oblique view. (a) Ti monomer, (b) Ti dimer, (c)-(d) Ti trimers. Top row: spin up; bottom row: spin down.

(7) Change in Spin-resolved PDOS of electron orbitals for Ti_n clusters

The bonding between Ti atom and substrate can be identified by the overlapped peaks of PDOS, as shown in Figs. S7(a)-(d). The PDOS of single Ti in Fig. S7(a)

shows that there is a larger overlap with the B_p orbital than with the N_p orbital, which agrees with the plot of Fig. 3(a) in the main text. Even when the Ti atoms of the dimer [Fig. S7(b)] or trimer [Figs. S7(c) and (d)] sit on top of the N atoms, the magnitude of N_p orbital peaks are less than one third of the corresponding B_p orbitals.

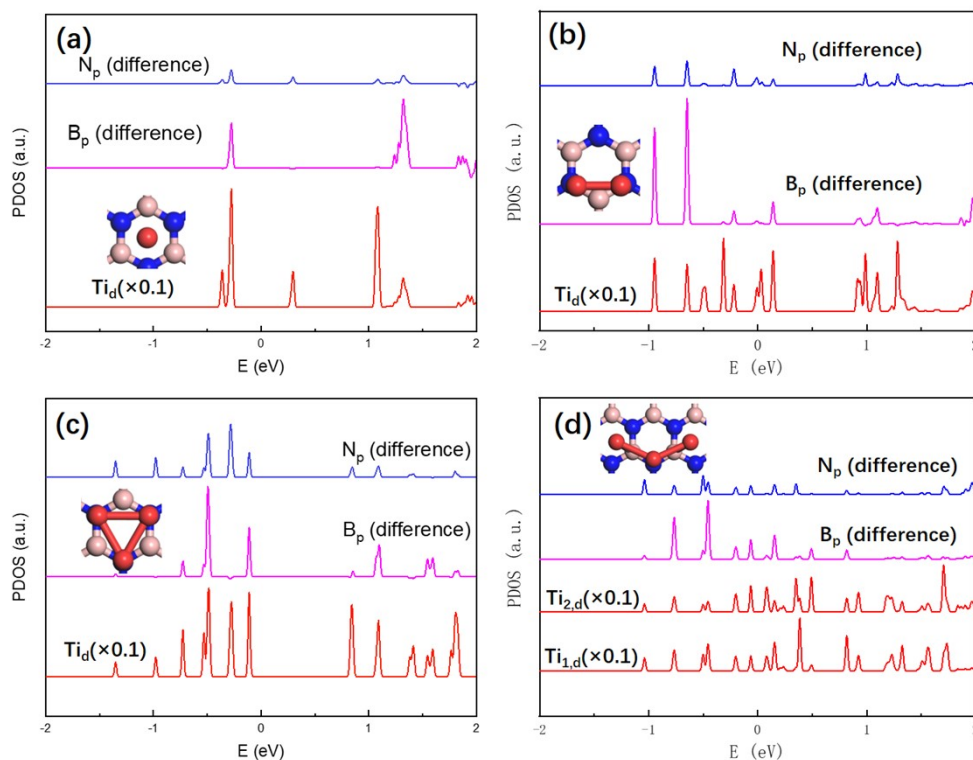
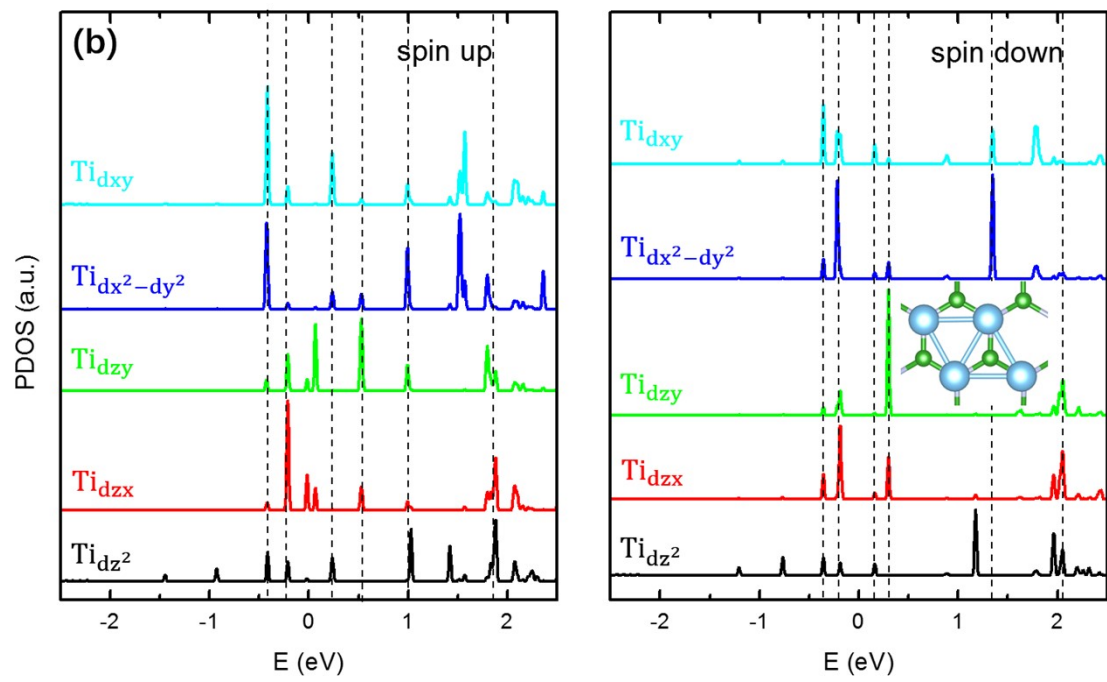
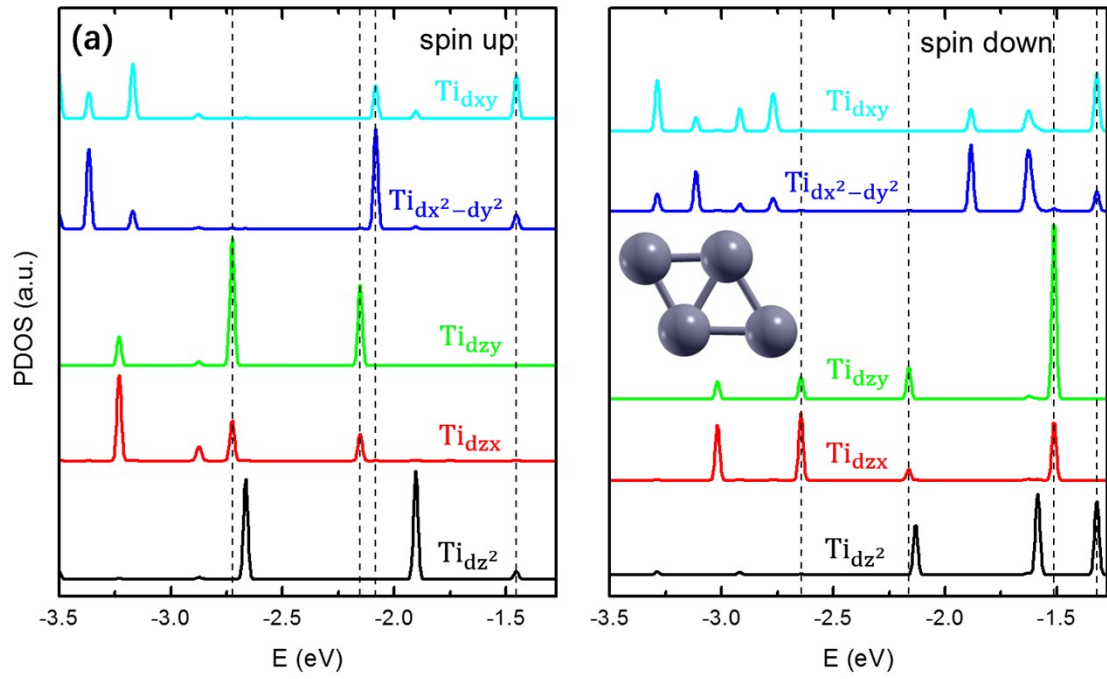


Figure S7. Projected density of states of Ti_n clusters, corresponding to the geometries of clusters in Fig. 1. Intensities of Ti atoms are divided by 10 to fit the plots. PDOS of N and B atoms are the difference between atoms in the adsorbed area and those in the unperturbed area. $Ti_{1,d}$ and $Ti_{2,d}$ represent the d orbital of Ti atoms in the middle and on the side of the cluster in (d).

(8) Comparison of projected density of states (PDOS) between isolated and adsorbed clusters



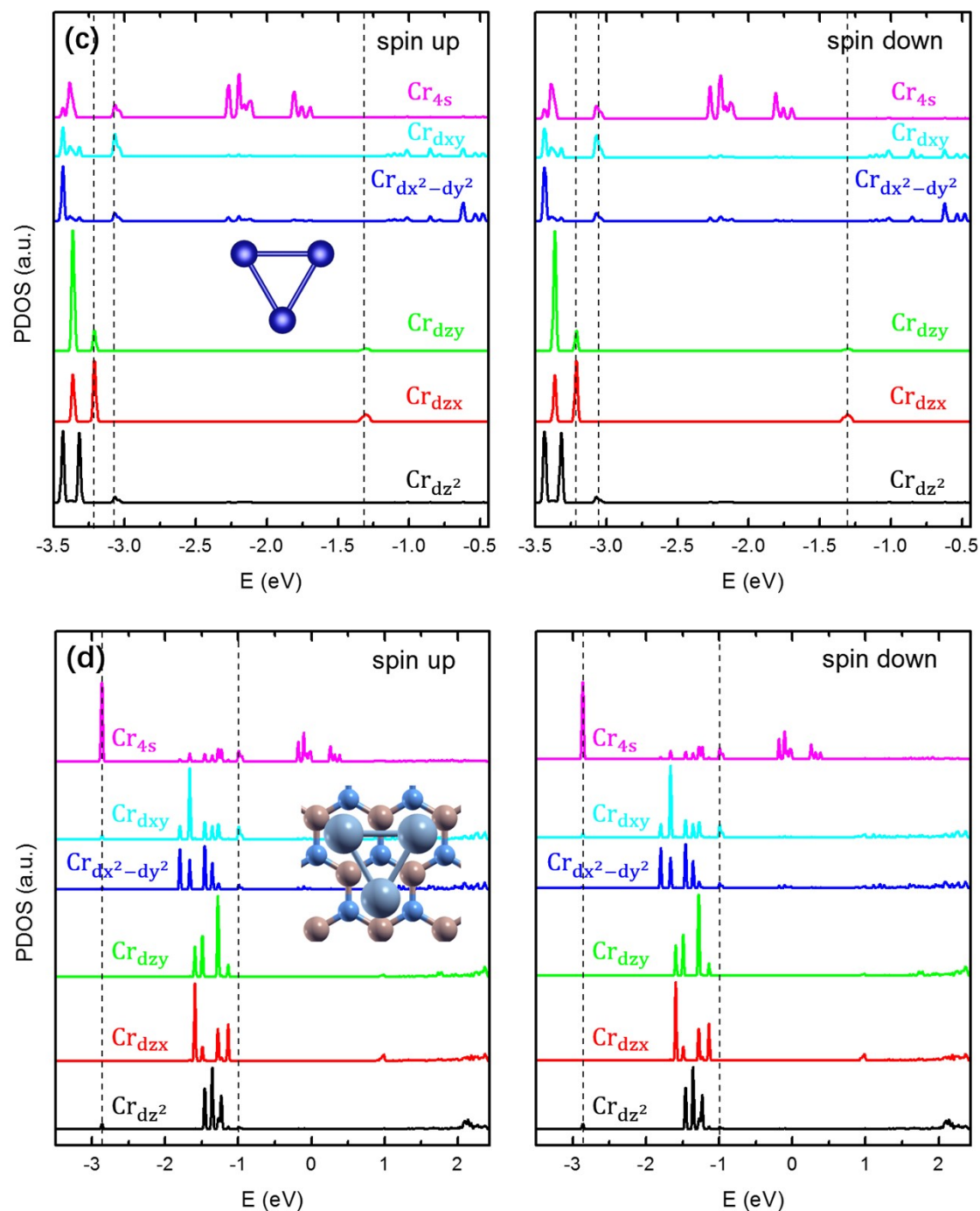


Figure S8. Comparison of spin-resolved PDOS of electron orbitals for Ti₄ [(a) and (b)] and Cr₃ [(c) and (d)] clusters between isolated and adsorbed clusters. For Cr₃, the underlying h-BN substrate results in shift of the sub-orbitals, whereas for Ti₄, additional hybridized orbitals emerge above -1.0 eV, besides the shift of Ti orbitals.

(9) HOMO and LUMO for Ti Clusters and BN Bandgap

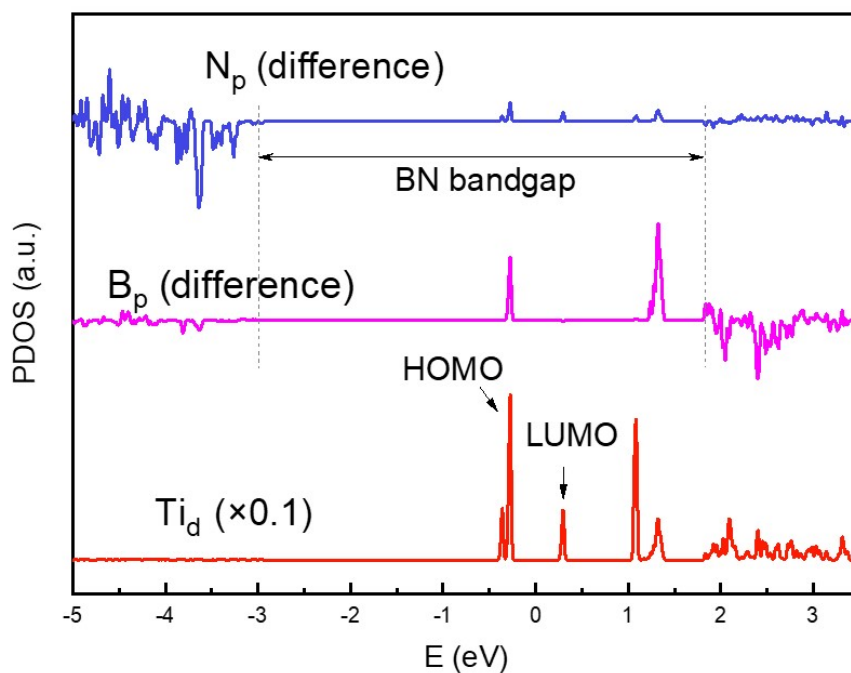


Figure S9. The bandgap of h-BN, as well as the top of the valence band and the bottom of the conduction band, derived from the partial density of states of the substrate. The HOMO and LUMO of Ti clusters are also marked in the partial density of states of the Ti atom.